In vivo single branch axotomy induces GAP-43–dependent sprouting and synaptic remodeling in cerebellar cortex

Anna Letizia Allegra Mascaro[a,1,2], Paolo Cesare[b,c,1,3], Leonardo Sacconi[a,d], Giorgio Grasselli[b,e], Georgia Mandolesi[b], Bohumil Maco[f], Graham W. Knott[f], Lieven Huang[g], Vincenzo De Paola[g], Piergiorgio Strata[b,c], and Francesco S. Pavone[a,d,h,i]

[a]European Laboratory for Non-Linear Spectroscopy, University of Florence, 50019 Sesto Fiorentino, Italy; [b]Fondazione Santa Lucia, Istituto di ricovero e cura a carattere scientifico (IRCCS), 00179 Rome, Italy; [c]National Institute of Neuroscience, University of Turin, 10125 Turin, Italy; [d]National Institute of Optics, National Research Council, 50125 Florence, Italy; [e]Department of Neurobiology, University of Chicago, Chicago, IL 60637; [f]Centre Interdisciplinaire de Microscopie Electronique, Ecole Polytechnique Federale de Lausanne, CH-1015 Lausanne, Switzerland; [g]Medical Research Council Clinical Science Centre, Faculty of Medicine, Imperial College London, W12 0NN London, United Kingdom; [h]Department of Physics, University of Florence, 50019 Sesto Fiorentino, Italy; and [i]International Center of Computational Neurophotonics, 50019 Sesto Fiorentino, Italy

Edited by Masao Ito, RIKEN Brain Science Institute, Wako, Japan, and approved May 15, 2013 (received for review November 7, 2012)

Plasticity in the central nervous system in response to injury is a complex process involving axonal remodeling regulated by specific molecular pathways. Here, we dissected the role of growth-associated protein 43 (GAP-43; also known as neuromodulin and B-50) in axonal structural plasticity by using, as a model, climbing fibers. Single axonal branches were dissected by laser axotomy, avoiding collateral damage to the adjacent dendrite and the formation of a persistent glial scar. Despite the very small denervated area, the injured axons consistently reshape the connectivity with surrounding neurons. At the same time, adult climbing fibers react by sprouting new branches through the intact surroundings. Newly formed branches presented varicosities, suggesting that new axons were more than just exploratory sprouts. Correlative light and electron microscopy reveals that the sprouted branch contains large numbers of vesicles, with varicosities in the close vicinity of Purkinje dendrites. By using an RNA interference approach, we found that downregulating GAP-43 causes a significant increase in the turnover of presynaptic boutons. In addition, silencing hampers the generation of reactive sprouts. Our findings show the requirement of GAP-43 in sustaining synaptic stability and promoting the initiation of axonal regrowth.

brain injury | two-photon imaging | neural plasticity | laser nanosurgery

The central nervous system (CNS) is capable of remodeling in response to various stimuli, like physiological experiences associated with adaptation, learning, and memory or pathological insults such as traumatic injuries (1, 2). The ability of adult neurons of the CNS to regenerate their axons in response to injury is limited in many neuronal types depending on both intrinsic and extrinsic factors (3–8). Axons in the CNS represent a challenging site for targeted manipulation and in vivo imaging, and little is known about their postlesional reactive plasticity and how this is regulated by molecular mediators. A full characterization of this dynamic process is a prerequisite for realizing successful brain repair.

Here, we investigated the reactive plasticity of an axonal terminal arbor by using climbing fibers (CFs) as a model. These axons were shown to retain a high regenerative potential also during adulthood (6, 9). The injury paradigms commonly used in previous studies, i.e., mechanical severing or chemical treatments, exhibit limited specificity while producing massive degeneration (10). In addition, postmortem analysis provides just snapshots of fixed tissue, not allowing an unambiguous distinction between regenerating and unaltered fibers at the lesion site (11, 12). Alternatively, in vitro studies lack the complexity of environmental cues that modulate the axonal response to injury.

Modern optical techniques have the potential to overcome these limitations (8, 13, 14). The restricted absorption volume and deep penetration of multiphoton excitation (15) can be used as a tool to dissect single neurites in the brain of adult mice in vivo (16). The severed neuron can be imaged by two-photon fluorescence (TPF) microscopy (17, 18), so that the reactive plasticity of the injured process can be monitored in optically accessible parts of the adult CNS in vivo. Based on these technologies, this study has analyzed the real-time structural dynamics and synaptic reorganization of a severed axon in the cerebellar cortex of adult mice, defining the timescale and extent of degeneration and remodeling in vivo. Here we show that our optical approach is able to ablate a single axonal branch avoiding collateral damage to the adjacent dendrite and the formation of a durable glial scar. We find that despite the very small denervated area, laser axotomy on single branches triggers axonal sprouting while eliciting synaptic remodeling in the surviving portion of the axon. Correlative light and electron microscopy reveals that the new varicosities formed on the sprouted branch lie next to Purkinje dendrites, and contain a large number of vesicles.

The plasticity of mature CFs has been frequently associated with the high basal expression of growth-associated proteins such as growth-associated protein 43 (GAP-43) (9, 19, 20). The involvement of GAP-43 in neuronal structural plasticity was demonstrated in many studies based on gene depletion or overexpression of its wild-type or mutated variants in cultured cells and transgenic mice (21, 22). GAP-43 overexpression is sufficient to induce neurite formation and axonal sprouting in different regions of adult CNS (21, 23, 24). However, the requirement of GAP-43 in both physiological and postinjury axonal dynamics has never been investigated. Because homozygous knock-out mice are affected by a very low-survival rate during the early postnatal period (<5%) (25, 26), we opted for an RNA-dependent gene-silencing approach. By delivering RNA-interfering lentiviral vectors in vivo, we down-regulated this gene specifically in CFs and without affecting brain development. We found that down-regulating GAP-

Author contributions: A.L.A.M., P.C., L.S., P.S., and F.S.P. designed research; A.L.A.M., P.C., L.S., G.G., G.M., B.M., G.W.K., L.H., and V.D.P. performed research; A.L.A.M., B.M., and G.W.K. analyzed data; and A.L.A.M., P.C., L.S., G.G., G.W.K., V.D.P., P.S., and F.S.P. wrote the paper.

The authors declare no conflict of interest.

This article is a PNAS Direct Submission.

Freely available online through the PNAS open access option.

[1]A.L.A.M. and P.C. contributed equally to this work.

[2]To whom correspondence should be addressed. E-mail: allegra@lens.unifi.it.

[3]Present address: Natural and Medical Sciences Institute at the University of Tubingen (NMI), 72770 Reutlingen, Germany.

This article contains supporting information online at www.pnas.org/lookup/suppl/doi:10.1073/pnas.1219256110/-/DCSupplemental.

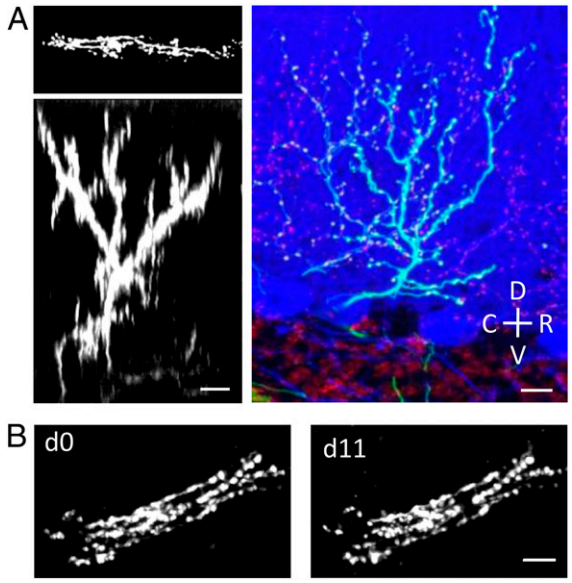

Fig. 1. In vivo imaging of CFs. (*A*) Two *Left* panels show the TPF transversal (maximum intensity *z*-projection of 60 images acquired from 0 to 120 μm deep below the pial surface) and sagittal view (digital rotation of the stack) of a single CF labeled by GFP expression in the cerebellar molecular layer. *Right* panel shows a confocal image of a single CF in a sagittal slice obtained from fixed cerebellum for comparison. CFs were labeled by GFP expression (green); Purkinje cells were labeled through immunofluorescent staining for Calbindin (in blue); CF varicosities in the molecular layer (together with some mossy fiber terminals in the granular layer) were labeled through immunofluorescent staining for VGlut2 (in red). C, caudal; D, dorsal; R, rostral; V, ventral. (*B*) Time-lapse images (TPF transversal view: maximum intensity *z*-projections) over a 12-d monitoring period showing the stability of CFs ascending branches. (Scale bar, 10 μm.)

43 profoundly affects the stability of varicosities and largely prevents the generation of reactive sprouts.

This study provides a unique in vivo description of axonal sprouting in the cerebellar system, shedding light on the role of GAP-43 in ensuring synaptic stability and promoting axonal regrowth after injury.

Results

Long-term structural plasticity of CFs was investigated by performing time-lapse TPF imaging on the cerebellar cortex of adult mice. The CFs were labeled with green fluorescent protein (GFP) following lentiviral injection in the inferior olive (IO). Three weeks after the injection, an optical window was chronically implanted on the cerebellar cortex. The viral injection produces a sparse labeling of CF, with variable levels of GFP expression (Fig. S1). A representative in vivo TPF image of a CF is shown in Fig. 1*A*. The CF terminal arbor is made by ascending branches, which are closely abutting the Purkinje cell (PC) dendritic arbor, and transverse branches (TBs), which are emerging perpendicularly from the ascending branches (27). As previously reported (28), the ascending branches display a high stability throughout the observation period of several days (Fig. 1*B*). Multiphoton laser axotomy was used to disrupt a single axonal branch. Highly localized damage was performed by irradiating a distal branch (ranging from 10 to 60 μm deep below the pia) of a labeled CF with a high energy dose of Ti:Sapphire laser. After laser irradiation, the distal part of the lesioned axon undergoes a sequence of swelling, degeneration, and disappearance (Fig. S2 and Fig. 2*A*). The specificity of this technique was explored by ablating an axonal branch and performing post hoc immunostaining of the PC dendrite adjacent to the axotomized CF. As shown in Fig. 2*B* we did not detect ($n = 9$) any visible degeneration of the PC dendrite at the lesion site. Because during laser-mediated brain injury, microglial processes may rapidly converge on the site of injury (29, 30), we quantified the density of microglia 1 d after the lesion. We found that our injury paradigm allows dissecting single axonal branches without inducing significant gathering of microglial cells near the site of injury (Fig. 2*C*).

The ability of injured nerve cells to compensate for the synaptic loss by modifying their connectivity with surrounding neurons is investigated in terms of structural rearrangement of presynaptic boutons. After laser axotomy, the surviving portions of the main arbor show a significant increase in the fraction of dynamic

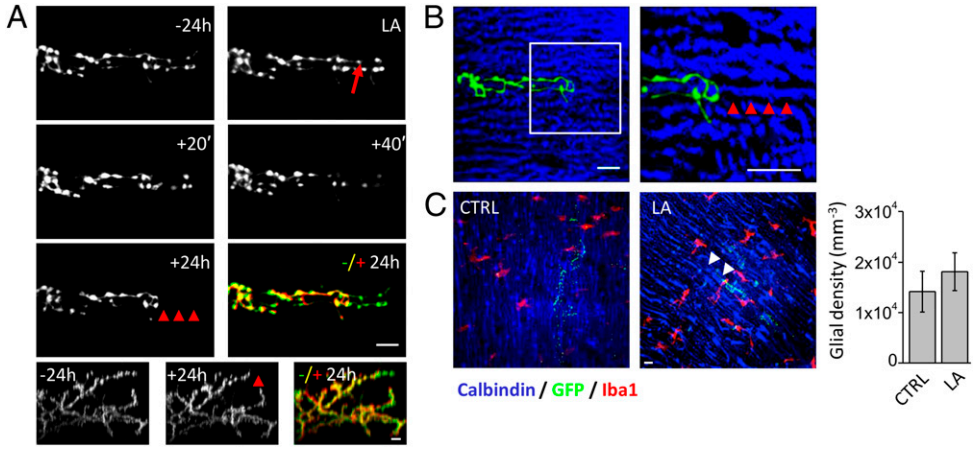

Fig. 2. In vivo multiphoton laser ablation of single axons. (*A*) Time course of a distal branch of a CF (TPF transversal view: maximum intensity *z*-projections) before (−24 h) and after laser axotomy (LA). The laser beam was focused on the axon where the red arrow points. Colored panel shows a superposition of the −24 h (green) and +24 h (red) frames. Red arrowheads at +24 h and the temporal merge highlight the degeneration of distal portion. *Lower* panels show sagittal views (digital rotation of the 3D TPF image) of the entire axonal arbor of the CF. (*B*) Confocal images of the same CF shown in *A* obtained from fixed cerebellum 1 d after laser axotomy. CFs (in green) are GFP labeled (maximum intensity *z*-projection from 0 to 88 μm below the pial surface); PCs (in blue) were labeled through immunofluorescent staining for Calbindin. The white box in *B* is shown magnified two times on the *Right* (maximum intensity *z*-projection of 8 μm). Red arrowheads highlight the integrity of the PC dendritic arbor within the region of the laser focus. (*C*) Confocal images showing CFs (in green), PCs (in blue), and microglial cells labeled through immunostaining for the anti-ionizing calcium-binding adaptor molecule 1 (Iba1) (in red) in a control region (CTRL) and around the lesion site (LA). White arrowheads in LA point at the region where the CF degenerated after laser axotomy. (Scale bar, 10 μm.) *Right* graph reports the density of microglial cells in CTRL ($N_{CF} = 9$) and around the lesion site (LA, $N_{CF} = 8$).

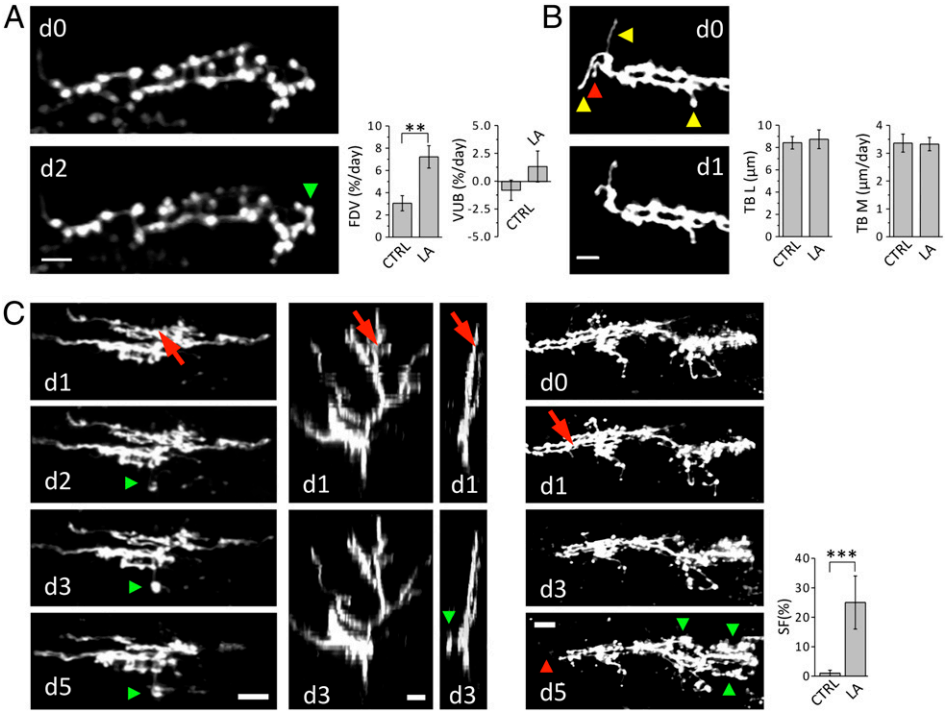

Fig. 3. Reactive plasticity of CFs after laser axotomy. (*A*) Time course of a portion of a CF showing the formation of a new varicosity (green arrowhead). (Scale bar, 5 μm.) Graphs compare average fractions of dynamic varicosities (FDVs) and the varicosities unbalance (VUB) in control animals (FDV = 3.1 ± 0.7% per day; VUB = −0.79 ± 0.91% per day; N_{Var} = 296, N_{CF} = 6) and in CFs injured by LA (FDV = 7.2 ± 1.0% per day; VUB = 1.34 ± 1.39% per day; N_{Var} = 433, N_{CF} = 6). $^{**}P < 0.01$ (two-tailed *t* test). (*B*) Time course of a portion of a CF displaying TB disappearance (red arrowhead) and remodeling (yellow arrowhead). Graphs compare TB length (TBL) and motility (TBM) in CTRL (TBL = 8.4 ± 0.5 μm; N_{TB} = 62, N_{CF} = 6; TBM = 3.4 ± 0.3 μm/d; N_{TB} = 94, N_{CF} = 6) and LA (TBL = 8.7 ± 0.8 μm; N_{TB} = 55, N_{CF} = 6; TBM = 3.3 ± 0.2 μm/d; N_{TB} = 131, N_{CF} = 6). (Scale bar, 5 μm.) (*C*) *Left* column images show the time course (from d1 to d5) of a CF after laser axotomy. The first image (d1) was acquired just before laser irradiation. The laser beam was focused on the axon where the red arrow points. Green arrowheads at d2, d3, and d5 highlight the protrusion of a new branch. Second and third column images show two orthogonal views (sagittal and coronal, respectively) of the same CF at d1 and d3. (Scale bar, 10 μm.) *Right* panels show another example of laser induced reactive plasticity. The first image (d0) was acquired 1 d before laser irradiation. The laser beam was focused on the axon at d1. Red and green arrowheads at d5 highlight the degeneration of the distal portion and the protrusion of new branches, respectively. (Scale bar, 15 μm.) Graph compares the sprouting frequency (SF) in CTRL (SF = 1 ± 1%; N_{CF} = 92, N_{mice} = 8) and LA (SF = 25 ± 9%; N_{CF} = 24, N_{mice} = 15). $^{***}P < 0.001$.

varicosities, without an overall variation of their total number (Fig. 3*A*). The degeneration of CF distal portion may alter the interaction and signaling between PC and CF, triggering synaptic rewiring on the surviving portion of the CF.

The CF arbor presents several transverse branches (TBs), thin filaments emerging perpendicularly from the main plane of the CF (27). The functional role of this pool of motile axons is still elusive. Previous studies proposed that dynamic TBs may be involved in regeneration or functional recovery (27, 28). This suggestion was based on the analogies between the TBs and the axonal filaments, similarly poor in varicosities, present in CFs sprouting branches (6). Our time-lapse observations show that in physiological conditions, TBs undergo rapid length changes in the time lapse of days (Fig. 3*B*). Although the mean length and motility of the TBs protruding from the injured fiber are not affected by laser axotomy (Fig. 3*B*), CFs can react to injury by sprouting new transverse axonal branches a few days (1–4) after laser axotomy (Fig. 3*C*). The new sprouts are significantly longer and brighter than preexisting TBs and do not stem from filaments present before axotomy. We find that sprouting of the injured CF can take place despite the very limited denervated area. No evident relation between the length of the degenerated axon and the length of the newly formed branch is observed (Fig. S3). The sprouted axon does not protrude toward the site left vacant by the injured CF branch, but in nearby regions where the PC should be normally innervated. Newly formed branches presented varicosities, suggesting that new axons may have some components of the neurotrasmitter release machinery (Fig. 4*A*). Using focused ion beam scanning electron microscopy (FIBSEM), we imaged a portion of a sprouted branch previously imaged in vivo (Fig. 4*B* and Movie S1), and 3 d after its appearance. We found the new axon contained mitochondria, endoplasmic reticulum, and large numbers of vesicles. These accumulated most in varicosities, which were found in close vicinity of Purkinje dendrites (Fig. 4*B*), suggestive of possible sites for synapse formation.

It has been proposed that the plasticity of mature CFs may be associated with their high basal expression of growth-associated proteins such as GAP-43 (9, 23). Using an in vivo RNAi approach to specifically down-regulate this protein in the IO, we investigated how the reduction in the expression of GAP-43 affects CFs synaptic remodeling and reactive plasticity. We found that silencing GAP-43 is sufficient to enhance the fraction of dynamic varicosities in CFs, with no variation in the overall density of varicosities (Fig. 5*A*). In line with previous works highlighting the importance of GAP-43 in regulating the stability of varicosities (22, 31), our results suggest a specific role for GAP-43 in maintaining the turnover of varicosities at a baseline level. Despite the structural modification induced by GAP-43 silencing in CFs varicosities, this does not affect TBs plasticity either in control conditions or in axotomized CFs (Fig. 5*B*). Similarly to what was observed in wild-type experiments, the reshaping of axonal connectivity in silenced mice increases even further following axotomy (Fig. 5*A*). This result indicates that the axotomy-induced increase in the turnover of varicosities is independent of GAP-43. On the other hand, sprouting of new

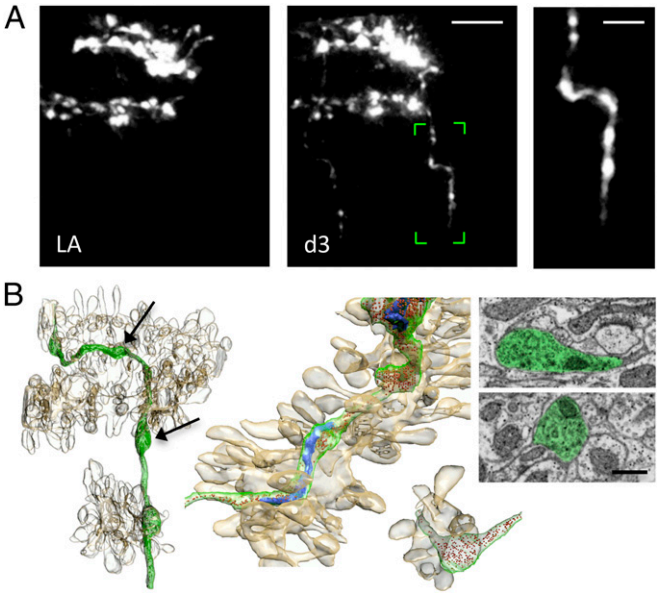

Fig. 4. Correlative light and electron microscopy of the sprouted axon. (*A*) Time course of a CF showing the formation of a new branch 3 d after laser axotomy in vivo. (Scale bar, 10 μm.) *Right* image shows the sprouted axon boxed (in green) in the *Center* panel with clearly visible varicosities along its length. (Scale bar, 5 μm.) (*B*) Block face scanning electron microscopy, using FIBSEM, of the same sprouted axon, enables its reconstruction in 3D (shown in green) along with its mitochondria in blue and the vesicles colored in red. Also reconstructed were the surrounding dendritic segments and their spines (light brown). *Center* shows magnified two details of the same reconstruction: *Top Left* image highlights the contiguity of the sprouted branch and the PC dendrite; the *Bottom Right* image emphasizes the close proximity of a varicosity to two dendritic spines. *Right*, electron micrographs from the series showing, pseudocolored in green, two varicosities containing vesicles and mitochondria, but no indications of synaptic contacts. Electron micrographs were collected at the level of two varicosities highlighted by black arrows. (Scale bar, 0.5 μm.)

branches in reaction to axotomy is severely impaired by the reduced expression of GAP-43 (Fig. 5*C*). This observation underlines an essential role played by GAP-43 in triggering the sprouting following injury in the adult brain, providing unique insights into the mechanism of axonal regrowth in vivo.

Discussion

In the present study, we investigated the real-time dynamics of axonal remodeling after laser axotomy. The high selectivity of this injury paradigm has been demonstrated by disrupting a single axonal branch without perturbing the conjugated PC dendrite. In fact, although we cannot exclude that laser irradiation may have triggered transient dendritic swelling or spine remodeling, we showed that the integrity of the PC dendritic arbor is maintained 1 d after the lesion. This highly localized damage does not trigger persistent microglial migration toward the lesion site. Although temporary transient effects cannot be discarded, one day after the lesion we did not detect microglia convergence on the site of injury. Our optical approach thus allows the paired investigation of pre- and postlesion axonal dynamics, avoiding long-lasting microglial activation and dendritic degeneration in a myelin-free environment.

Previous studies have shown that CFs are highly plastic and may expand or retract depending on available denervated target or on target removal, respectively (9). In this respect, we do not observe significant variation in the average length and motility of TBs in the injured axon, and none of the monitored TBs resulted to be buds of sprouted branches. Nevertheless, the surviving portion of the axotomized CF reacts by protruding new branches in the same direction of TBs. Indeed, the sprouted axon elongate in a region where PCs should be regularly innervated. We reconstructed the sprouted branch previously imaged in vivo with focused ion beam scanning electron microscopy. Three days after its appearance, the new axon contained some components of the synaptic machinery. The newly formed varicosities lay next to Purkinje dendrites and gather a high density of vesicles, resembling developing sites for synapse formation.

A reshape in axonal connectivity is revealed by an increase in the turnover of varicosities on the portion of the injured CF not involved in remodeling events such as degeneration or sprouting. The focal lesion promotes synaptic reorganization on the entire CF, which possibly plays a compensatory role after damage.

Thus far we have shown that our approach can unravel the time-lapse dynamics of axonal degeneration, sprouting and synaptic remodeling. We wondered if one or a few molecular promoters intrinsic to the CF were responsible for activating the sprouting program. The intrinsic ability of CFs to regrow has often been associated with the growth-associated protein GAP-43. Our in vivo observations in normally developed animals show that down-regulating GAP-43 profoundly affects the stability of varicosities, eliciting an overall increase in the fraction of dynamic varicosities. This is consistent with the proposed role played by GAP-43 in the adult CNS in neurotransmitter release and synaptic plasticity (31–38).

The requirement of GAP-43 in axonal plasticity was further demonstrated in our injury paradigm. Although the average motility of TBs is not affected, nor did we observe a general atrophy of these structures, down-regulation of GAP-43 prevents the generation of reactive sprouts in laser axotomized CFs. Our results suggest that GAP-43 mediates the initiation of postinjury axonal outgrowth.

Axonal degeneration and modifications in GAP-43 expression profiles are associated with a plethora of neurological diseases, including amyotrophic lateral sclerosis, multiple sclerosis, epilepsy, diabetic neuropathy, schizophrenia, and Alzheimer's and Parkinson diseases (39–43). In this respect, the results and techniques presented here may be helpful in assessing and validating new therapeutic strategies to prevent degeneration and promote axonal regrowth (44, 45).

Materials and Methods

In Vivo Labeling of CFs and GAP-43 Silencing. Lentiviral vectors encoding GFP (kindly provided by Luigi Naldini, San Raffaele Hospital, Milan, Italy), either alone or in tandem with a shRNA sequence targeting GAP-43 (namely siGAP) were prepared and injected as recently described (31). Briefly, the virus was injected into the IO of adult (9–12 wk) wild-type Friend leukemia virus B (FVB) mice (Harlan) after deep anesthesia by i.p. injection of ketamine (90 mg/kg) and xylazine (9 mg/kg). The muscles on the dorsal neck were retracted to expose the dura over the foramen magnum, and an opening was then made in the dura to expose the brainstem. Injections were made unilaterally at the midline, at the midpoint between the caudal edge of the cerebellar cortex and the first cervical vertebra, at a depth of 1.6 mm. Injections were made by a borosilicate capillary set at an angle 50° from vertical. A volume of viral suspension of 0.1–0.3 μL was delivered over a 6- to 12-min period. The pipettes were left in place for 15 min before they were withdrawn.

Open Skull Technique. Two to 3 wk after the viral injection, a craniotomy was performed above the vermis and the lateral hemispheres of the cerebellum. The mice were deeply anesthetized as described above. To minimize swelling at the site of surgery, a small dose of dexamethasone (0.04 mL at 2 mg/mL) was administrated before the procedure. A semicircular portion of the skull (4 mm diameter) above the cerebellar cortex was removed and the exposed region was then covered with a coverglass and sealed with dental cement. To minimize the inflammatory phenomena that may take place after the surgery, the mice were treated daily with carprofen (5 mg/kg). The craniotomy does not induce significant microglial activation (Fig. S4), consistent with previous work (46). The experimental protocols were designed in accordance with the rules of the Italian Ministry of Health.

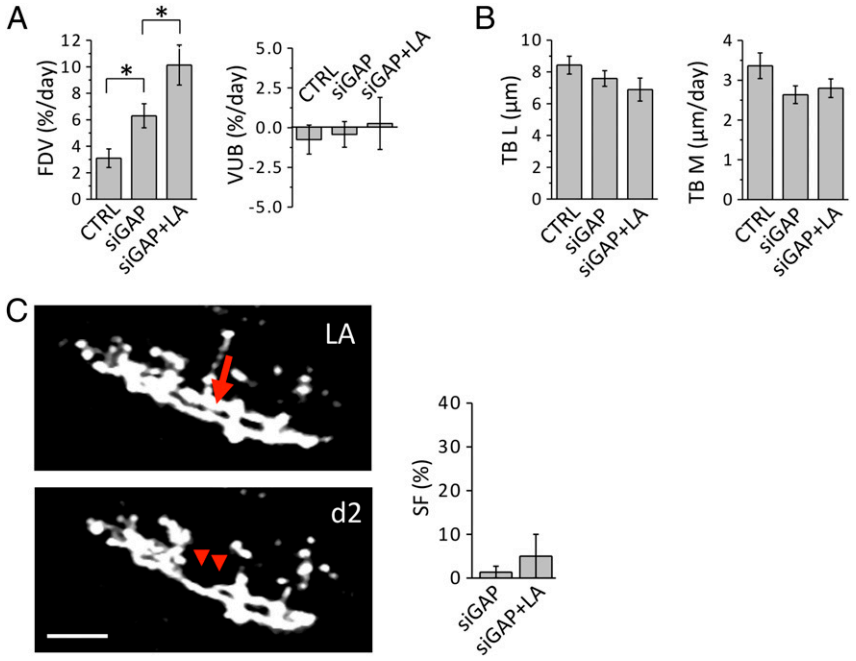

Fig. 5. Role of GAP-43 in axonal plasticity. (*A*) Graphs compare the FDV and VUB for wild type (CTRL), GAP-43 silenced (siGAP; FDV = 6.3 ± 0.9% per day; VUB = −0.47 ± 0.81% per day; $N_{Var} = 486$, $N_{CF} = 7$), and siGAP laser axotomized CFs (siGAP + LA; FDV = 10.1 ± 1.5% per day; VUB = 0.22 ± 1.64% per day; $N_{Var} = 500$, $N_{CF} = 6$). *$P < 0.05$. (*B*) Graphs compare TB length (TBL) and motility (TBM) in wild type (CTRL), GAP-43 silenced CFs (siGAP; TBL = 7.6 ± 0.5 µm; $N_{TB} = 38$, $N_{CF} = 6$; TBM = 2.6 ± 0.2 µm; $N_{TB} = 89$, $N_{CF} = 6$) and siGAP laser axotomized CFs (siGAP + LA; TBL = 6.9 ± 0.7 µm; $N_{TB} = 53$, $N_{CF} = 6$; TBM = 2.8 ± 0.2 µm; $N_{TB} = 130$, $N_{CF} = 6$). (*C*) Time course of a CF in a siGAP animal displaying the degeneration of a CF (red arrowheads) after LA, but no sprouting. (Scale bar, 15 µm.) Graph compares the SF in SiGAP (SF = 1.3 ± 1.3%; $N_{CF} = 74$, $N_{mice} = 5$) and siGAP laser axotomized (SF = 5 ± 5%; $N_{CF} = 9$, $N_{mice} = 6$) CFs.

In Vivo Imaging and Laser Axotomy. The basic design of our TPF imaging system has already been described (16). Briefly, a mode-locked Ti:Sapphire laser (Chameleon; Coherent) (120-fs width pulses, 90-MHz repetition rate) was coupled into a custom-made scanning system based on a pair of galvanometric mirrors (VM500; GSI Lumonics). The laser was focused onto the specimen by a physiology objective (XLUM 20, NA 0.95, WD 2 mm; Olympus). A closed-loop piezoelectric stage (P-721; Physik Instrumente) was used for axial displacements of the objective. The fluorescence signal was collected by a photomultiplier module (H7710-13; Hamamatsu Photonics). The same experimental setup was used for imaging and for laser axotomy. Laser axotomy was performed by irradiating with a high-energy dose of Ti:Sapphire laser a selected point on a distal portion of a CF. In a typical experiment, the laser power was increased 5–10 times more than the power used for imaging and the laser shutter was opened for a period of the order of hundreds of milliseconds. The wavelength used for laser axotomy was the same chosen for imaging (935 nm). For more details regarding the laser surgery procedure, see ref. 47. The reactive plasticity of irradiated CFs was monitored daily by TPF 3D imaging. Three-dimensional stacks (2-µm *z*-axis step) were acquired from the pia mater down to a depth of around 200 µm, setting a field of view of 100 × 100 μm^2 and a resolution of 512 × 512 $pixel^2$. During imaging and laser axotomy sessions, the mice were lightly anesthetized for a period of ∼90 min.

Immunohistochemistry. After the last in vivo imaging session, the animals were deeply anesthetized as described above and intracardiacally perfused with 4% (wt/vol) paraformaldehyde in 0.1 M phosphate buffer (pH 7.4). Brains were postfixed overnight at 4 °C. Transversal sections 60 µm thick were incubated overnight at 4 °C with mouse monoclonal anti-calbindin D28K 1:2,000 (Swant), rabbit polyclonal Iba 1 antibody 1:1,000 (Wako Chemicals), or anti-VGluT2 1:500 (Synaptic Systems). After washing, sections were incubated for 2 h at room temperature (RT) with 1:200 Alexa 633 anti-mouse (Invitrogen), and Alexa 532 anti-rabbit (Invitrogen). Images from immunolabeled samples were acquired with a 63× (1.4 NA) oil immersion objective and a Leica confocal imaging system (Leica; TCS SP5). Glial activation was quantified by measuring the density of glial cells, i.e., the number of glial cells on the analyzed cortical volume (200 × 200 × 20 μm^3).

Three-Dimensional Electron Microscopy of Imaged Axons. To image the sprouting axon with electron microscopy, we used a correlative approach with the block face scanning method of focused ion beam scanning electron microscopy (46). Immediately after the last in vivo imaging session, the animals were deeply anesthetized, as described above, and intracardiacally perfused with 2% paraformaldehyde and 2.5% glutaraldehyde in 0.1 M phosphate buffer (pH 7.4). Sections of 60-µm thickness were then cut, using a vibratome, tangential to the surface of the cerebellum, and parallel to the imaging plane of the TPF microscope. These were then imaged and a small (30 × 30 μm^2) square was burned with the laser, around the region of interest (48). This fiducial mark was then visible after resin embedding and used to locate the imaged axon. The section was then stained with 1.5% (wt/vol) potassium ferrocyanide and 1% (wt/vol) osmium tetroxide in 0.1 M cacodylate buffer (0.1 M, pH 7.4) followed by 1% (wt/vol) uranyl acetate, and then dehydrated with ethanol and embedded in Durcupan resin. Once the resin was cured, the region of interest was then cut from the rest of the section, stuck to a blank resin block, and trimmed with an ultramicrotome so that the laser region of interest was ∼5 µm below the surface. This was then placed on a metal stub, gold coated in a plasma vaporation system (Cressington), and placed inside a FIBSEM (Zeiss; NVision 40) (48). This was used to image the face of the block at exactly the position above the laser marks. A total of 2,700 serial images were collected, with 12-nm distance between each image. The pixel size was 6 nm. The image stack was visualized using FIJI software, and the axon found by searching at the position measured in relation to the laser marks, and compared with the fluorescent images taken of the fixed section when the marks were made. The axon was segmented in the TrakEM2 module using the FIJI software (49), and included in this were the dendrites of the nearby Purkinje neurons. The model was then exported to Blender, a 3D modeling program, for the final rendering (www.blender.org).

Image Analysis. TPF 3D stacks were analyzed through ImageJ software. First, the 3D TPF stacks were preprocessed through a median filter to reduce the shot noise in each optical frame. Axonal swellings bigger than 0.6 μm^2 and two times brighter than the adjacent axonal backbone were scored as varicosities. The CFs varicosities were analyzed comparing two maximum intensity *z*-projections acquired on the boundary of the monitoring period (ranging from 5 to 17 d). For the laser axotomized CFs, we compared the image acquired just before the irradiation with that acquired the last monitoring day. We first tried a day-by-day analysis of varicosities. Due to the high intrinsic stability found by this preliminary investigation, a time-course analysis on varicosities was considered redundant. The fraction of dynamic varicosities (FDV) was calculated as the sum of the percentage variation of the newly appeared

and disappeared varicosities, normalized by the number of imaging days. The varicosity unbalance (VUB) was calculated as the difference between the fractions of newly formed and disappeared varicosities, normalized by the number of imaging days. TB length measurement was performed through a frame-by-frame analysis of the 3D stacks. Axonal filaments perpendicular to the main branch longer than 2 μm were scored as TBs. TB length was measured from the edge of the ascending branch to the fiber tip through a manually superimposed segmented line. The accuracy of the operator on TB length measurement was quantified (SD of the mean) ~0.2 μm. The calculation of the mean length values was performed by averaging TB length of the same experimental group [control, (CTRL) and laser axotomy (LA)] choosing the first imaged day for physiological conditions and the last for laser axotomized CFs. TB motility (TBM) was calculated averaging the root mean square (RMS) velocity of each TB of the same experimental group. RMS velocity was calculated by measuring TB length variation during days (ranging from 5 to 17 d). For the laser axotomized CFs, the RMS was calculated starting from the irradiation day. The morphological changes of ascending branches were investigated through a time-series analysis. The appearance of a new branch was scored as a sprouting event if the new portion was as bright as the main CF arbor, and was longer than 10 μm. The sprouting frequency (SF) is the number of sprouting axons normalized on the total number of imaged CFs for each experimental group. Unless otherwise stated, data are reported as mean ± SEM. The mean and SEM of LA in siGAP animals (Fig. 5*C*) are calculated by the Wilson score interval (experimental values of the binomial distribution: $n = 9$, $P = 0$). Statistical differences between experimental groups are verified by the unpaired *t* test, and are considered significant when $P < 0.05$.

ACKNOWLEDGMENTS. We thank Dr. Francesco Vanzi and Ferdinando Rossi for helpful discussions on the manuscript; Ludovico Silvestri for discussions on image analysis; Vladimiro Batocchi for technical assistance; Prof. Luigi Naldini for the lentiviral vector; and Graham Little, Luca Mazzoni, and Raffaele Coppini for assistance with immunohistochemical analysis. The research leading to these results has received funding from LASERLAB-EUROPE (Grant 284464, European Commission's Seventh Framework Programme). This research project has also been supported by the Italian Ministry for Education, University and Research in the framework of the Flagship Project NANOMAX and by Italian Ministry of Health in the framework of the "Stem Cells Call for Proposals." This work is part of the research activities of the European Flasghip Human Brain Project and has been carried out in the framework of the International Center of Computational Neurophotonics foundation supported by "Ente Cassa di Risparmio di Firenze."

1. Buonomano DV, Merzenich MM (1998) Cortical plasticity: From synapses to maps. *Annu Rev Neurosci* 21:149–186.
2. Ruediger S, et al. (2011) Learning-related feedforward inhibitory connectivity growth required for memory precision. *Nature* 473(7348):514–518.
3. Tuszynski MH, Steward O (2012) Concepts and methods for the study of axonal regeneration in the CNS. *Neuron* 74(5):777–791.
4. Horner PJ, Gage FH (2000) Regenerating the damaged central nervous system. *Nature* 407(6807):963–970.
5. Snider WD, Zhou FQ, Zhong J, Markus A (2002) Signaling the pathway to regeneration. *Neuron* 35(1):13–16.
6. Rossi F, Wiklund L, van der Want JJ, Strata P (1991) Reinnervation of cerebellar Purkinje cells by climbing fibres surviving a subtotal lesion of the inferior olive in the adult rat. I. Development of new collateral branches and terminal plexuses. *J Comp Neurol* 308(4):513–535.
7. Hawthorne AL, et al. (2011) The unusual response of serotonergic neurons after CNS Injury: Lack of axonal dieback and enhanced sprouting within the inhibitory environment of the glial scar. *J Neurosci* 31(15):5605–5616.
8. Kerschensteiner M, Schwab ME, Lichtman JW, Misgeld T (2005) In vivo imaging of axonal degeneration and regeneration in the injured spinal cord. *Nat Med* 11(5):572–577.
9. Carulli D, Buffo A, Strata P (2004) Reparative mechanisms in the cerebellar cortex. *Prog Neurobiol* 72(6):373–398.
10. Buffo A, Fronte M, Oestreicher AB, Rossi F (1998) Degenerative phenomena and reactive modifications of the adult rat inferior olivary neurons following axotomy and disconnection from their targets. *Neuroscience* 85(2):587–604.
11. Cafferty WBJ, McGee AW, Strittmatter SM (2008) Axonal growth therapeutics: Regeneration or sprouting or plasticity? *Trends Neurosci* 31(5):215–220.
12. Steward O, Zheng B, Tessier-Lavigne M (2003) False resurrections: Distinguishing regenerated from spared axons in the injured central nervous system. *J Comp Neurol* 459(1):1–8.
13. Bhatt DH, Otto SJ, Depoister B, Fetcho JR (2004) Cyclic AMP-induced repair of zebrafish spinal circuits. *Science* 305(5681):254–258.
14. Misgeld T, Kerschensteiner M (2006) In vivo imaging of the diseased nervous system. *Nat Rev Neurosci* 7(6):449–463.
15. Zipfel WR, Williams RM, Webb WW (2003) Nonlinear magic: Multiphoton microscopy in the biosciences. *Nat Biotechnol* 21(11):1369–1377.
16. Sacconi L, et al. (2007) In vivo multiphoton nanosurgery on cortical neurons. *J Biomed Opt* 12(5):050502.
17. Helmchen F, Denk W (2005) Deep tissue two-photon microscopy. *Nat Methods* 2(12): 932–940.
18. Svoboda K, Yasuda R (2006) Principles of two-photon excitation microscopy and its applications to neuroscience. *Neuron* 50(6):823–839.
19. Kruger L, Bendotti C, Rivolta R, Samanin R (1993) Distribution of GAP-43 mRNA in the adult rat brain. *J Comp Neurol* 333(3):417–434.
20. Grasselli G, Strata P (2013) Structural plasticity of climbing fibers and the growth-associated protein GAP-43. *Front Neural Circuits* 7:25.
21. Buffo A, et al. (1997) Targeted overexpression of the neurite growth-associated protein B-50/GAP-43 in cerebellar Purkinje cells induces sprouting after axotomy but not axon regeneration into growth-permissive transplants. *J Neurosci* 17(22):8778–8791.
22. Mosevitsky MI (2005) Nerve ending "signal" proteins GAP-43, MARCKS, and BASP1. *Int Rev Cytol* 245:245–325.
23. Aigner L, et al. (1995) Overexpression of the neural growth-associated protein GAP-43 induces nerve sprouting in the adult nervous system of transgenic mice. *Cell* 83(2): 269–278.
24. Zhang Y, et al. (2005) Growth-associated protein GAP-43 and L1 act synergistically to promote regenerative growth of Purkinje cell axons in vivo. *Proc Natl Acad Sci USA* 102(41):14883–14888.
25. Maier DL, et al. (1999) Disrupted cortical map and absence of cortical barrels in growth-associated protein (GAP)-43 knockout mice. *Proc Natl Acad Sci USA* 96(16): 9397–9402.
26. Strittmatter SM, Fankhauser C, Huang PL, Mashimo H, Fishman MC (1995) Neuronal pathfinding is abnormal in mice lacking the neuronal growth cone protein GAP-43. *Cell* 80(3):445–452.
27. Sugihara I, Wu H, Shinoda Y (1999) Morphology of single olivocerebellar axons labeled with biotinylated dextran amine in the rat. *J Comp Neurol* 414(2):131–148.
28. Nishiyama H, Fukaya M, Watanabe M, Linden DJ (2007) Axonal motility and its modulation by activity are branch-type specific in the intact adult cerebellum. *Neuron* 56(3):472–487.
29. Davalos D, et al. (2005) ATP mediates rapid microglial response to local brain injury in vivo. *Nat Neurosci* 8(6):752–758.
30. Nimmerjahn A, Kirchhoff F, Helmchen F (2005) Resting microglial cells are highly dynamic surveillants of brain parenchyma in vivo. *Science* 308(5726):1314–1318.
31. Grasselli G, Mandolesi G, Strata P, Cesare P (2011) Impaired sprouting and axonal atrophy in cerebellar climbing fibres following in vivo silencing of the growth-associated protein GAP-43. *PLoS ONE* 6(6):e20791.
32. Dekker LV, De Graan PNE, Oestreicher AB, Versteeg DHG, Gispen WH (1989) Inhibition of noradrenaline release by antibodies to B-50 (GAP-43). *Nature* 342(6245): 74–76.
33. Neve RL, et al. (1998) The neuronal growth-associated protein GAP-43 interacts with rabaptin-5 and participates in endocytosis. *J Neurosci* 18(19):7757–7767.
34. Haruta T, Takami N, Ohmura M, Misumi Y, Ikehara Y (1997) Ca2+-dependent interaction of the growth-associated protein GAP-43 with the synaptic core complex. *Biochem J* 325(Pt 2):455–463.
35. Riederer BM, Routtenberg A (1999) Can GAP-43 interact with brain spectrin? *Brain Res Mol Brain Res* 71(2):345–348.
36. Gianotti C, Nunzi MG, Gispen WH, Corradetti R (1992) Phosphorylation of the presynaptic protein B-50 (GAP-43) is increased during electrically induced long-term potentiation. *Neuron* 8(5):843–848.
37. Ramakers GMJ, et al. (1995) Temporal differences in the phosphorylation state of pre- and postsynaptic protein kinase C substrates B-50/GAP-43 and neurogranin during long-term potentiation. *J Biol Chem* 270(23):13892–13898.
38. Ramakers GMJ, McNamara RK, Lenox RH, De Graan PNE (1999) Differential changes in the phosphorylation of the protein kinase C substrates myristoylated alanine-rich C kinase substrate and growth-associated protein-43/B-50 following Schaffer collateral long-term potentiation and long-term depression. *J Neurochem* 73(5):2175–2183.
39. Conforti L, Adalbert R, Coleman MP (2007) Neuronal death: Where does the end begin? *Trends Neurosci* 30(4):159–166.
40. Raff MC, Whitmore AV, Finn JT (2002) Axonal self-destruction and neurodegeneration. *Science* 296(5569):868–871.
41. Stokin GB, et al. (2005) Axonopathy and transport deficits early in the pathogenesis of Alzheimer's disease. *Science* 307(5713):1282–1288.
42. Oestreicher AB, De Graan PN, Gispen WH, Verhaagen J, Schrama LH (1997) B-50, the growth associated protein-43: modulation of cell morphology and communication in the nervous system. *Prog Neurobiol* 53(6):627–686.
43. Teunissen CE, et al. (2006) Growth-associated protein 43 in lesions and cerebrospinal fluid in multiple sclerosis. *Neuropathol Appl Neurobiol* 32(3):318–331.
44. Canty AJ, et al. (2013) In-vivo single neuron axotomy triggers axon regeneration to restore synaptic density in specific cortical circuits. *Nature Comm*, 10.1038/ncomms3038.
45. Canty AJ, et al. (2013) Synaptic elimination and protection after minimal injury depend on cell type and their pre-lesion structural dynamics in the adult cerebral cortex. *J Neurosci*, 10.1523/JNEUROSCI.0254-13.2013.
46. Holtmaat A, et al. (2009) Long-term, high-resolution imaging in the mouse neocortex through a chronic cranial window. *Nat Protoc* 4(8):1128–1144.
47. Allegra Mascaro AL, Sacconi L, Pavone FS (2010) Multi-photon nanosurgery in live brain. *Front Neuroenergetics* 2:21.
48. Maco B, et al. (2013) Correlative in vivo 2 photon and focused ion beam scanning electron microscopy of cortical neurons. *PLoS ONE* 8(2):e57405.
49. Cardona A, et al. (2012) TrakEM2 software for neural circuit reconstruction. *PLoS ONE* 7(6):e38011.